JACS
JOURNAL OF THE AMERICAN CHEMICAL SOCIETY

Communication

pubs.acs.org/JACS

Electrocatalytic Hydrogen Redox Chemistry on Gold Nanoparticles

Mathias Brust*[,†] and Gabriel J. Gordillo*[,‡]

[†]Department of Chemistry, University of Liverpool, Crown Street, Liverpool L69 7ZD, United Kingdom

[‡]Departamento de Química Inorgánica, Analítica y Química Física, Facultad de Ciencias Exactas y Naturales, INQUIMAE (CONICET), Universidad de Buenos Aires, Ciudad Universitaria, Pabellón 2 (1428), Buenos Aires, Argentina

Supporting Information

ABSTRACT: Electrocatalytic proton reduction leading to the formation of adsorbed molecular hydrogen on gold nanoparticles of 1−3 and 14−16 nm diameter stabilized by 1-mercapto-undecane-11-tetra(ethyleneglycol) has been demonstrated by cyclic voltammetry using a hanging mercury drop electrode. The nanoparticles were adsorbed to the electrode from aqueous dispersion and formed robust surface layers transferrable to fresh base electrolyte solutions. Unique electrocatalytic proton redox chemistry was observed that has no comparable counterpart in the electrochemistry of bulk gold electrodes. Depending on size, the nanoparticles have a discrete number of electrocatalytically active sites for the two-electron/two-proton reduction process. The adsorbed hydrogen formed is oxidized with the reverse potential sweep. These findings represent a new example of qualitative different behavior of nanoparticles in comparison with the corresponding bulk material.

Gold is one of the most important metals in nanotechnology, primarily due to the exceptional ambient stability of nanostructures made from it. Further appeal stems from its plasmonic properties, the ease of surface functionalization by well-established gold−thiol chemistry and, not least, the surprising catalytic activity of nanometric gold, which is not exhibited by macroscopic gold surfaces.[1] Since Haruta's landmark discovery of low temperature catalytic oxidation of carbon monoxide at oxide-supported gold nanoparticles, catalysis has become one of the fastest growing lines of gold nanoparticle research.[2] Electrochemistry as a means of charging gold nanoparticles has extensively been used since Murray's pioneering work on quantized capacitance charging.[3] Recently, Tsukuda and co-workers demonstrated that aerobic oxidation catalysis by gold is possible in the absence of a support material.[4] Using gold nanoparticles stabilized by poly(*N*-vinyl-2-pyrrolidone) (PVP) in both aqueous and organic media, their work also established that polymer protection of nanoparticles does not necessarily poison their catalytic activity. While most research in this area, so far, has focused on oxidations, Mirkhalaf and Schiffrin have recently demonstrated electrocatalytic oxygen reduction by surface immobilized gold nanoparticles capped by a hydrophobic organic monolayer.[5] Gold nanoparticles are also known to adsorb molecular hydrogen, which is not observed at surfaces of bulk gold and is of great importance for the development of new hydrogenation catalysts.[6] A density functional theory study by Barrio et al. suggests that this can be attributed to the presence of low coordinated Au atoms, high fluxionality and cooperation between active Au atoms in the clusters.[7]

Related to these previous findings, we report here highly unusual electrochemical properties of water-dispersible ligand-stabilized gold nanoparticles studied by cyclic voltammetry (CV) on a hanging mercury drop electrode in aqueous electrolyte. For this purpose, gold nanoparticles of two different size ranges, 1−3 and 14−16 nm, were prepared by well-established methods (see SI 1 for experimental details). Particle stability and dispersibility in water was achieved by the choice of the ligand, 1-mercapto-undecane-11-tetra(ethyleneglycol). For electrochemical characterization, particles of each size range were added as aqueous dispersions to an acetic acetate buffer solution (0.1 M, pH 4.5) that served as the base electrolyte, to give a final gold content of 0.1 g/L. A freshly generated hanging mercury drop served as working electrode, which was polarized with respect to a Ag|AgCl 3.5 M reference electrode using a platinum wire as counter electrode. For comparison with bulk gold, a gold disk electrode was used instead of the mercury drop as working electrode in pure base electrolyte. Before all measurements, oxygen was purged from the solution with nitrogen. Cyclic voltammograms of the hanging mercury drop electrode in pure base electrolyte (baseline) and in a dispersion of 1−3 nm gold nanoparticles, and of the gold disk electrode in pure base electrolyte, are shown in Figure 1. The baseline shows that in the absence of the gold nanoparticles, no electroactive species is present that could be reduced or oxidized within the chosen potential range. The gold disk electrode shows the typical well-known behavior of bulk gold surfaces in this potential range with reductive hydrogen evolution toward the cathodic end of the potential sweep as the only salient feature. At the hanging drop electrode this feature is absent due to the high over potential for hydrogen evolution on mercury, making this electrode an ideal substrate to study metal particles in this potential range. After addition of the 1−3 nm particles, a prominent reduction and corresponding oxidation peak appear in the cyclic voltammogram and massive hydrogen evolution now occurs toward the cathodic limit of the potential sweep. In addition, a small constant cathodic current is observed negative of the reduction peak. This cyclic voltammogram is reproducible and stable over hundreds of cycles except for some poorly defined very small undulations at potentials negative of the reduction peak.

Received: October 24, 2011
Published: January 27, 2012

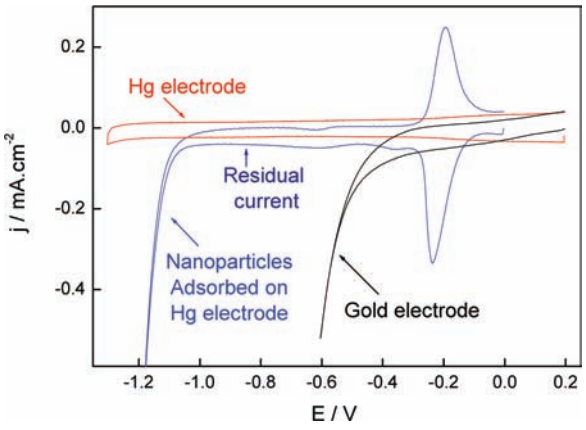

Figure 1. Cyclic voltammetric response of a dispersion of 1−3 nm gold nanoparticles (gold content 0.1 g/L) at a hanging mercury drop electrode in aqueous acetic acetate buffer (0.1 M, pH 4.5) at a potential sweep rate of 1 V s^{-1} (blue line). Gold disk (black line) and hanging mercury drop (red line) electrode under the same conditions but in the absence of nanoparticles. All potentials were measured against a AglAgCl 3.5 M reference electrode and are quoted against NHE.

The observed peaks show a linear dependence of the peak currents on the potential sweep rate (see SI 2), which confirms that the reduction and oxidation processes involved are surface bound and not diffusion controlled. If instead of the 1−3 nm particles a preparation of 14−16 nm gold particles is added, virtually the same electrochemical behavior is obtained, while the addition of particle free supernatant fluids from nanoparticle preparations has no effect on the baseline.

Also, the ligand, 1-mercapto-undecane-11-tetra-(ethyleneglycol), on its own, while expected to form a self-assembled monolayer on the mercury surface, does not show any electrochemical activity in the potential range of interest here. It is therefore concluded that the new features appearing upon addition of gold nanoparticles are attributable to the electrochemical activity of the particles themselves.

If the electrode is removed from the solution containing the nanoparticles and immersed in a fresh base electrolyte solution all features attributed to the particles are fully retained, indicating that the particles form a robust film on the mercury surface. Even if a fresh mercury drop is created in fresh base electrolyte solution, rudiments of the redox peak characteristic of the particles remain and only disappear completely after several fresh mercury drops have been produced. This indicates that the nanoparticle film does not only form on the exposed mercury surface but also leaches into the capillary at the glass mercury interface. Another clear indication of film formation by the gold nanoparticles is the characteristic feature of hydrogen evolution at the cathodic limit of the cyclic voltammogram, which is not observed on the clean mercury electrode. Its onset is negatively shifted by about 600 mV with respect to hydrogen evolution on bulk gold. The assumption that a complete monolayer of nanoparticles is formed on the electrode surface is supported by the observation that for both particle sizes the peak current rapidly approaches a constant saturation value after immersion of the electrode. We attribute the adsorptive behavior of the particles to the adaptive properties of the amphiphilic ligand, which enables the particle to expose either hydrophilic or hydrophobic moieties and hence facilitates adhesion to the hydrophobic mercury surface in contact with water. Film formation is also readily observed with the naked eye, for example on the hydrophobic surfaces of plastic centrifuge tubes. On the contrary, purely hydrophilic gold nanoparticles, we found, do not adsorb to plastic or mercury and show no distinctive electrochemistry on mercury electrodes.

The key challenge that arises from the above observations is to identify the new electrochemical redox process associated with the presence of the gold nanoparticle film. Since both small and large particles give practically identical results although they were prepared by very different methods, and neither their supernatant solutions nor the ligand alone are electrochemically active, it is concluded that the redox process takes place at the remaining accessible metal surface of the adsorbed gold nanoparticles. A hypothetical reaction that could account for our observations is the reduction and oxidation of Au(I) surface sites on the particles. This interpretation, however, would suggest no, or little, dependence of the redox potential on the pH value of the electrolyte solution since protons do not participate in the reaction. In order to test this, the mercury drop electrode was immersed for a few seconds is an aqueous dispersion of gold nanoparticles (gold content ~0.5 g/L) to form a surface film (both size ranges gave the same result) and then transferred to a freshly prepared buffer solution of exactly adjusted pH value. The potential between the reduction and the oxidation peaks was taken as the equilibrium redox potential of the redox couple under investigation. The particle film on the electrode was so robust, that all measurements involving buffer solutions of five different pH values could be made with one film without measurable loss of particles. As shown in Figure 2, the redox potential depends

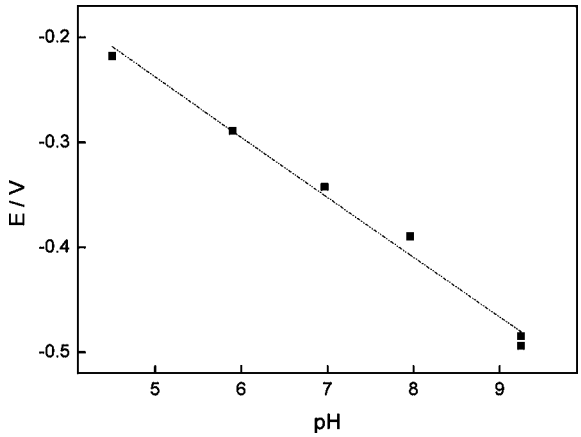

Figure 2. pH dependence of redox potential taken as the medium value between cathodic and anodic peak potential. These results were obtained by pre-adsorption of 14−16 nm gold nanoparticles to a hanging mercury drop electrode and successive immersion in aqueous buffer solutions of determined pH value. All potentials were measured against a AglAgCl 3.5 M reference electrode and are quoted against NHE.

linearly on the pH value of the electrolyte solution and systematically shifts to more positive values with increasing proton concentration by 58 mV per pH unit. This indicates that protons take part in this reaction and are consumed in the reduction process and generated in the oxidation step. The theoretically expected change in redox potential for such a reaction is 59.1 mV per pH unit, i.e., very close to our

dx.doi.org/10.1021/ja2096514 | J. Am. Chem. Soc. 2012, 134, 3318−3321

experimental value. Hence, it is unlikely that reduction of Au(I) sites is involved in this process.

It is therefore concluded that the electrochemical surface process observed here is the reversible electrocatalytic reduction of protons to form an adsorbed hydrogen species. The related oxidation peak on the reverse sweep conversely corresponds to the re-oxidation of the adsorbed hydrogen species. At bulk gold electrodes, the existence of two distinct mechanisms of proton reduction followed by hydrogen evolution is well-accepted: (i) reductive proton adsorption followed immediately by surface combination of two adsorbed hydrogen atoms and release of molecular hydrogen (one-electron process, Volmer–Tafel mechanism), and (ii) reductive proton adsorption followed immediately by reduction of a second proton at the same site and release of molecular hydrogen (two-electron process, Volmer–Heyrovsky mechanism).[8,9] In contrast to the behavior observed here for nanoparticles, at bulk gold electrodes neither of the two mechanisms leads to the build-up of detectable amounts of adsorbed species. In order to determine which underlying type of mechanism is likely to be dominant in the present case, it is necessary to establish whether it is a one- or a two-electron transfer reaction. This can be achieved by relating the peak current density, J_p, to the charge transferred, Q, and it can also be inferred from the half peak width, $\Delta E_{p/2}$, which is expected to be $90.6/n$ mV, where n is the number of electrons transferred. Both diagnostic tests in the present case indicate a sequential two-electron transfer reaction, i.e., the predominance of a nanoscale variant of the Volmer–Heyrovsky mechanism resulting in the formation of adsorbed molecular hydrogen according to eq 1 (see SI 3 for a detailed analysis and the result of a numerical simulation of the CV).

$$\mathrm{Au} + \mathrm{H}^+ + e^- \rightarrow \mathrm{Au-H} \quad (1a)$$

$$\mathrm{Au-H} + \mathrm{H}^+ + e^- \rightarrow \mathrm{Au} + \mathrm{H_2} \quad (1b)$$

For different mercury drops the mean value for the charge per unit electrode area corresponding to the integrated peak under saturation conditions was 17 ± 1 μC cm^{-2}. The area under the peak is proportional to the number of protons reduced and oxidized, respectively, and allows estimating the number of active sites per nanoparticle provided the number of nanoparticles adsorbed to the electrode is known. Assuming hexagonal close packing of spherical particles with interdigitation of part of the ligand shell, the number of particles per unit electrode area is estimated to be 4×10^{11} cm^{-2} for particles of 14–16 nm diameter, and 7.2×10^{12} cm^{-2} for the 2–3 nm particles. From this follows that, on average, a 14–16 nm particle has about 130 active sites for hydrogen reduction to form adsorbed hydrogen molecules, while the 2–3 nm particles each have about 10 sites. Given that the surface area of the large particles is about 50-fold that of the small ones, the density of active sites is about 4 times higher on the small particles. This is not unexpected since smaller particles have a higher number of exposed atomic sites, while most surface atoms on larger particles are within facets as in surfaces of bulk metal. Given the very similar behavior of particles of both size ranges, it is likely that the observed hydrogen reduction is due to the electrode geometry rather than being an electronic size effect. With increasing electrode size the relative number of active sites decreases, so that bulk electrodes do no longer show detectable reactivity.The relatively small number of active sites may also be an explanation for the absence of the one-electron reduction mechanism followed by surface recombination of adsorbed atomic hydrogen. The sites are likely to be spaced too far from each other for this process to occur, and hence the alternative two-electron reduction is observed, which does not require surface mobility of adsorbed hydrogen. A similar hindrance of the recombination of adsorbed atomic hydrogen has been observed before when alkane thiols were adsorbed to gold nanoparticles already covered with organic sulphides.[10] Finally, the small constant current observed negative of the peak potentials in both potential scanning directions we interpret as a steady state release of hydrogen from the hydrogen saturated surface of the nanoparticles. The measured current density of 20 μA cm^{-2} corresponds to a production rate of molecular hydrogen of 1×10^{-10} mol s^{-1} cm^{-2}. This gives an average turn over rate at each reaction site of 1.7 s^{-1} for the 2–3 nm particles and 0.5 s^{-1} for the 14–16 nm ones. The poorly reproducible slight undulation in this current may be due to a minority of ligands being reorganized or reductively desorbed.

The separation between anodic and cathodic peak increases not only with increasing sweep rate (SI 4) as usually the case for quasi-reversible systems, but also with increasing surface coverage of nanoparticles on the Hg drop electrode, as shown in Figure 3. This indicates that the electron transfer kinetics

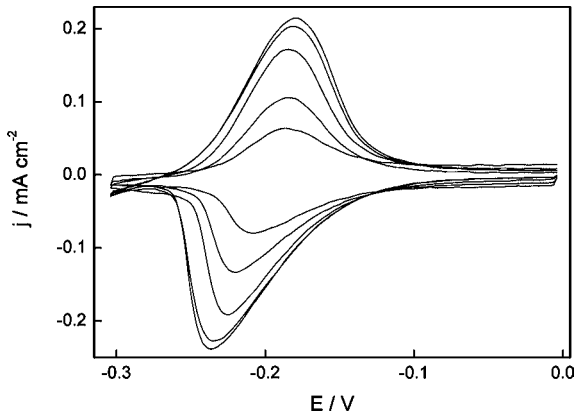

Figure 3. Cyclic voltammetric response of a growing surface film of 14–16 nm gold nanoparticles at a hanging mercury drop electrode in aqueous acetic acetate buffer (0.1M, pH 4.5) at a potential sweep rate of 1 V s^{-1}. Five successive voltammograms are shown with increasing peak current densities representing increasing surface coverage of the electrode as the gold nanoparticles are being adsorbed to finally reach a saturation value (monolayer coverage). Note the increasing peak separation with increasing coverage. All potentials were measured against a AgIAgCl 3.5 M reference electrode and are quoted against NHE.

slightly slow down with increasing particle coverage. The resulting peak distortion is much more pronounced for the cathodic reaction, which may be due to the increased crowding of ligands that make the access of the second proton to the reaction site more difficult and hence increases the electron transfer resistance. The anodic peak would be less affected since the electroactive species is already adsorbed to the particle. This effect is even more pronounced when the mercury drop electrode is first modified with an adsorbed layer of gold nanoparticles by immersion in a dispersion of a gold content of ~0.5 mg/L, and then transferred to a fresh solution of base electrolyte (SI 5). The peak separation is now markedly increased with an even stronger distortion of the cathodic peak, while the maximum peak current obtainable and the

dx.doi.org/10.1021/ja2096514 | J. Am. Chem. Soc. 2012, 134, 3318–3321

corresponding maximum charge that can be transferred remain the same. We tentatively attribute this to the formation of particle multilayers from the more concentrated dispersion, of which only the one directly adjacent to the mercury electrode is electrochemically active.

This interpretation is also consistent with our measurements of the pH dependence of the equilibrium redox-potential, which was carried out by immersing the same electrode covered with pre-adsorbed particles in electrolyte solutions of different pH. In each case it took a few seconds until the new equilibrium potential was obtained, indicating that the pH equilibrium between the reaction site and the bulk solution is established relatively slowly compared to the time scale of a typical CV experiment (SI 6). This would be expected if the active part of the electrode is covered by a nanoparticle multilayer film.

Two important questions remain to be addressed: (i) what is the role of mercury as an electrode material, and (ii) is thiol-protection of the particles needed to achieve the observed behavior? In order to demonstrate that the use of mercury is helpful but not essential to observe hydrogen adsorption and desorption peaks on gold nanoparticles we modified a gold electrode in an alternate fashion with nonanedithiol and with 15 nm citrate-stabilized gold particles to build up five subsequent layers of nanoparticles spaced by nonanedithiol.[11] The proton peaks characteristic of gold nanoparticles, albeit cathodically shifted, are clearly present in this system, which demonstrates that the presence of mercury is not essential for this behavior to be observed (SI 7). This experiment also suggests that thiol termination is not essential to observe reductive hydrogen adsorption since the active top layer of particles was not thiolated, except for its anchorage to the preceding layer. Furthermore, preliminary experiments with bismuth film electrodes instead of mercury also show proton adsorption peaks.

In conclusion, we have described a remarkable difference between the electrochemical properties of bulk gold electrodes and thiol-protected gold nanoparticles of two different size ranges. In contrast to bulk gold, nanoparticles exhibit electrocatalytic formation of adsorbed molecular hydrogen. Our findings are of fundamental interest and in agreement with recent computational studies and experimental findings of hydrogen adsorption on gold nanoparticles. They also generate opportunities for new applied research in electrocatalysis, hydrogenation catalysis and electroanalytical chemistry. The gold nanoparticle, unexpectedly, has its own distinct electrochemical signature, clearly observable at least at a mercury electrode. This is of diagnostic value and can be used to detect the presence of the particles electrochemically without the need for an electro-active tag.

■ ASSOCIATED CONTENT

Ⓢ Supporting Information

SI 1, materials and preparation of gold nanoparticles; SI 2, linear dependence of anodic and cathodic peak currents on potential sweep rate; SI 3, mechanistic analysis and digital simulation; SI 4, dependence of peak potentials on the log of the sweep rate; SI 5, cyclic voltammogram obtained with preadsorbed multilayer of gold particles at pH 4.5; SI 6, two successive cyclic voltammograms obtained with pre-adsorbed multilayer of gold particles after changing the buffer from pH 4.5 to 5.9; SI 7, cyclic voltammograms of clean gold electrode and gold electrode that has been modified with five successively attached layers of citrate-stabilized 14−16 nm gold particles in acetic−acetate buffer of pH 4.5. This material is available free of charge via the Internet at http://pubs.acs.org.

■ AUTHOR INFORMATION

Corresponding Author

M.Brust@liv.ac.uk; gabriel@qi.fcen.uba.ar

Notes

The authors declare no competing financial interest.

■ ACKNOWLEDGMENTS

The authors are grateful recipients of a Royal Society Joint Project Grant. G.J.G. is member of the National Research Council of Argentina (CONICET).

■ REFERENCES

(1) (a) Astruc, D. *Chem. Rev.* **2004**, *104*, 293−346. (b) Hutchings, G. J.; Brust, M.; Schmidbaur, H. *Chem. Soc. Rev.* **2008**, *37*, 1759−1765. (c) Myroshnychenko, V.; Rodríguez-Fernández, J.; Pastoriza-Santos, I.; Funston, A. M.; Novo, C.; Mulvaney, P.; Liz-Marzán, L. M.; García De Abajo, F. J. *Chem. Soc. Rev.* **2008**, *37*, 1792−1805. (d) Herzing, A. A.; Kiely, C. J.; Carley, A. F.; Landon, P.; Hutchings, G. J. *Science* **2008**, *321*, 1331−1335.

(2) (a) Haruta, M.; Kobayashi, T.; Sano, H.; Yamada, N. *Chem. Lett.* **1987**, 405−408. (b) Haruta, M.; Yamada, N.; Kobayashi, T.; Iijima, S. *J. Catal.* **1989**, *115*, 301−309. (c) Haruta, M. *Catal. Today* **1997**, *36*, 153−166.

(3) (a) Ingram, R. S.; Hostetler, M. J.; Murray, R. W.; Schaaff, T. G.; Khoury, J. T.; Whetten, R. L.; Bigioni, T. P.; Guthrie, D. K.; First, P. N. *J. Am. Chem. Soc.* **1997**, *119*, 9279−9280. (b) Chen, S.; Ingram, R. S.; Hostetler, M. J.; Pietron, J. J.; Murray, R. W.; Schaaff, T. G.; Khoury, J. T.; Alvarez, M. M.; Whetten, R. L. *Science* **1998**, *280*, 2098−2101. (c) Chen, S.; Murray, R. W.; Feldberg, S. W. *J. Phys. Chem. B* **1998**, *102*, 9898−9907. (d) Murray, R. W. *Chem. Rev.* **2008**, *108*, 2688−2720.

(4) (a) Tsunoyama, H.; Ichikuni, N.; Sakurai, H.; Tsukuda, T. *J. Am. Chem. Soc.* **2009**, *131*, 7086−7093. (b) Tsukuda, T.; Tsunoyama, H.; Sakurai, H. *Chem.—Asian J.* **2011**, *6*, 736−748.

(5) Mirkhalaf, F.; Schiffrin, D. J. *Langmuir* **2010**, *26*, 14995−15001.

(6) (a) Claus, P. *Appl. Catal., A* **2005**, *291*, 222−229. (b) Kartusch, C.; van Bokhoven, J. A. *Gold Bull.* **2009**, *42*, 343−348.

(7) Barrio, L.; Liu, P.; Rodríguez, J. A.; Campos-Martín, J. M.; Fierro, J. L. G. *J. Chem. Phys.* **2006**, *125*, 164715.

(8) (a) Brug, G. J.; Sluyters-Rehbach, M.; Sluyters, J. H. *J. Electroanal. Chem.* **1984**, *181*, 245−266. (b) Hamelin, A.; Weaver, M. J. *J. Electroanal. Chem.* **1987**, *223*, 171−184.

(9) Vetter, K. J. *Electrochemical Kinetics*; Academic Press: New York, 1967.

(10) Hasan, M.; Bethell, D.; Brust, M. *J. Am. Chem. Soc.* **2002**, *124*, 1132−1133.

(11) (a) Bethell, D.; Brust, M.; Schiffrin, D. J.; Kiely, C. J. *J. Electroanal. Chem.* **1996**, *409*, 137−143. (b) Brust, M.; Bethell, D.; Kiely, C. J.; Schiffrin, D. J. *Langmuir* **1998**, *14*, 5425−5429.